Inorg. Chem. **2003**, *42*, 3925–3933

Nickel Complexes of *o*-Amidochalcogenophenolate(2−)/*o*-Iminochalcogenobenzosemiquinonate(1−) π-Radical: Synthesis, Structures, Electron Spin Resonance, and X-ray Absorption Spectroscopic Evidence

Chung-Hung Hsieh,[†,‡] I-Jui Hsu,[§] Chien-Ming Lee,[‡] Shyue-Chu Ke,*[,∥] Tze-Yuan Wang,[§] Gene-Hsiang Lee,[§] Yu Wang,*[,§] Jin-Ming Chen,[⊥] Jyh-Fu Lee,[⊥] and Wen-Feng Liaw*[,‡]

Department of Chemistry, National Tsing Hua University, Hsinchu 30043, Taiwan, Department of Chemistry, National Taiwan University, Taipei, Taiwan, Department of Chemistry, National Changhua University of Education, Changhua, Taiwan, Department of Physics, National Dong Hwa University, Hualien, Taiwan, and Synchroton Radition Research Center, Hsinchu 30077, Taiwan

Received February 25, 2003

The preparation of complexes *trans*-[Ni(−SeC_6H_4-*o*-NH−)$_2$]$^-$ (**1**), *cis*-[Ni(−TeC_6H_4-*o*-NH−)$_2$]$^-$ (**2**), *trans*-[Ni(−SC_6H_4-*o*-NH−)$_2$]$^-$ (**3**), and [Ni(−SC_6H_4-*o*-S−)$_2$]$^-$ (**4**) by oxidative addition of 2-aminophenyl dichalcogenides to anionic [Ni(CO)$(SePh)_3$]$^-$ proves to be a successful approach in this direction. The *cis* arrangement of the two tellurium atoms in complex **2** is attributed to the intramolecular Te···Te contact interaction (Te···Te contact distance of 3.455 Å). The UV–vis electronic spectra of complexes **1** and **2** exhibit an intense absorption at 936 and 942 nm, respectively, with extinction coefficient ϵ > 10000 L mol^{-1} cm^{-1}. The observed small *g* anisotropy, the principal *g* values at $g_1 = 2.036$, $g_2 = 2.062$, and $g_3 = 2.120$ for **1** and $g_1 = 2.021$, $g_2 = 2.119$, and $g_3 = 2.250$ for **2**, respectively, indicates the ligand radical character accompanied by the contribution of the singly occupied d orbital of Ni(III). The X-ray absorption spectra of all four complexes show L_{III} peaks at ∼854.5 and ∼853.5 eV. This may indicate a variation of contribution of the Ni(II)–Ni(III) valence state. According to the DFT calculation, the unpaired electron of complex **1** and **2** is mainly distributed on the $3d_{xz}$ orbital of the nickel ion and on the $4p_z$ orbital of selenium (tellurium, $5p_z$) as well as the $2p_z$ orbital of nitrogen of the ligand. On the basis of X-ray structural data, UV–vis absorption, electron spin resonance, magnetic properties, DFT computation, and X-ray absorption (K- and L-edge) spectroscopy, the monoanionic *trans*-[Ni(−SeC_6H_4-*o*-NH−)$_2$]$^-$ and *cis*-[Ni(−TeC_6H_4-*o*-NH−)$_2$]$^-$ complexes are appositely described as a resonance hybrid form of Ni(III)–bis(*o*-amidochalcogenophenolato(2−)) and Ni(II)–(*o*-amidochalcogenophenolato(2−))–(*o*-iminochalcogenobenzosemiquinonato(1−) π-radical; i.e., complexes **1** and **2** contain delocalized oxidation levels of the nickel ion and ligands.

Introduction

The recent reports on the preparations of the varieties of five-coordinated 16-electron transition-metal complexes [M$(CO)_n(CN)_{3-n}$(−EC_6H_4-*o*-E′−)]$^-$ (M = Mn,[1,2] Fe,[3] W, Cr, Mo;[4] E = O, S, Se, Te; E′ = O, S, NH; *n* = 3, 2) revealed that [−EC_6H_4-*o*-E′−]$^{2-}$ acted as a strong π-bonding bidentate ligand, which allowed a rationalization of the short M−E/M−E′ bond lengths and simultaneously proved the importance of π-bonding for stabilization of the unsaturatedly

* Authors to whom correspondence should be addressed. E-mail: wfliaw@mx.nthu.edu.tw (W.-F.L.); yuwang@xtal.ch.ntu.edu.tw (Y.W.); ke@mail.ndhu.edu.tw (S.-C.K.).
† National Changhua University of Education.
‡ National Tsing Hua University.
§ National Taiwan University.
∥ National Dong Hwa University.
⊥ Synchroton Radition Research Center.

(1) (a) Liaw, W.-F.; Hsieh, C.-K.; Lin, G.-Y.; Lee, G.-H. *Inorg. Chem.* **2001**, *40*, 3468. (b) Liaw, W.-F.; Lee, C.-M.; Lee, G.-H.; Peng, S.-M. *Inorg. Chem.* **1998**, *37*, 6396.
(2) Hartl, F.; Vlcék, A., Jr.; deLearie, L. A.; Pierpont, C. G. *Inorg. Chem.* **1990**, *29*, 1073.
(3) Liaw, W.-F.; Lee, N.-H.; Chen, C.-H.; Lee, C.-M.; Lee, G.-H.; Peng, S.-M. *J. Am. Chem. Soc.* **2000**, *122*, 488.
(4) (a) Darensbourg, D. J.; Draper, J. D.; Reibenspies, J. H. *Inorg. Chem.* **1997**, *36*, 3648. (b) Darensbourg, D. J.; Klausmeyer, K. K.; Reibenspies, J. H. *Inorg. Chem.* **1996**, *35*, 1535.

10.1021/ic034211r CCC: $25.00
Published on Web 05/15/2003

Scheme 1

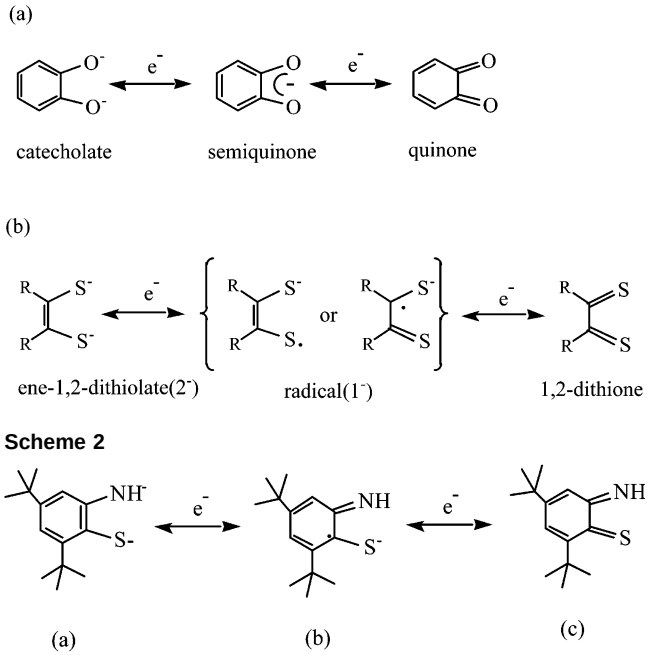

Scheme 2

coordinated $[M(CO)_n(CN)_{3-n}(-EC_6H_4\text{-}o\text{-}E'-)]^-$ systems.[1−4] The existence of one π-bond and two σ-bonds between the $[Mn(CO)_3]^+$ and $[-SC_6H_4\text{-}o\text{-}S-]^{2-}$ fragments, based on the qualitative frontier molecular orbital analysis,[5] also indicated that the lone-pair electrons are delocalized among the sulfur−manganese−sulfur system to stabilize the five-coordinate complex $[Mn(CO)_3(-SC_6H_4\text{-}o\text{-}S-)]^-$.[5] In fact, the analogous catecholate and dithiolene ligands have long been suggested to behave as "noninnocent" ligands to exhibit different oxidation levels (catecholate(−2), semiquinone(−1), quinone-(0), ene-1,2-dithiolate(−2), and semidithione radical(−1), 1,2-dithione(0), respectively) as shown in Scheme 1a[6] and b,[7] respectively. Although the iron complexes of *o*-benzenedithiolate ($[bdt]^{2-}$) indicate that $[bdt]^{2-}$ behaves as an innocent dithiolate based on crystal X-ray diffraction and Mössbauer spectra, it is still ascribed as the formation of dithio-*o*-benzoquinone which breaks up the aromatic system.[8]

Interestingly, the recent investigation of the nickel, palladium, and platinum complexes of *o*-amidothiophenolates shows that *o*-amidothiophenolate also acts as a "noninnocent" ligand which can exist at three different oxidation levels, *o*-amidothiophenolato(2−) (Scheme 2a), the *o*-iminothionebenzosemiquinonato(1−) π-radical (Scheme 2b), and *o*-iminothionequinone (Scheme 2c).[9] Meanwhile, the structural and spectroscopic criteria have been developed to address the presence of *o*-iminothionebenzosemiquinonato(1−) π-radicals in transition-metal complexes and to identify the oxidation level of metal ions and ligands.[9]

Scheme 3

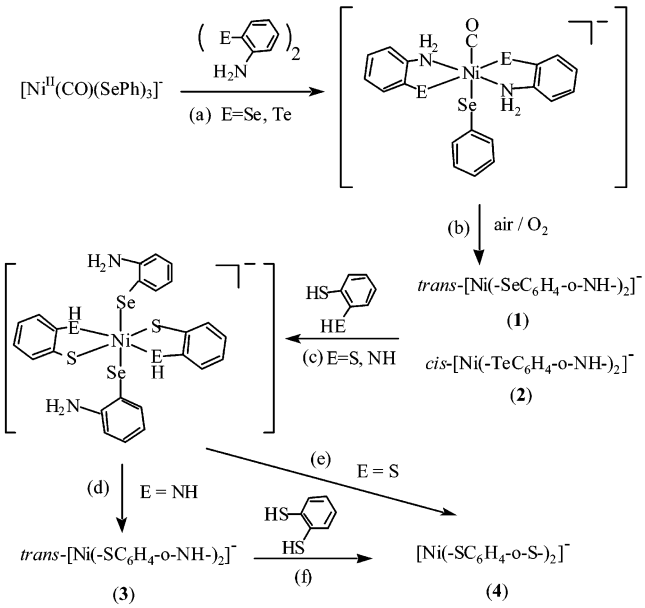

The present work was undertaken in order to expand the scope of transition-metal *o*-amidochalcogenophenolato derivatives. It may provide valuable evidence concerning the delocalized oxidation levels of the metal ion and ligands (resonance hybrid complexes)[9] and certainly will provide comparisons among transition-metal *o*-amidochalcogenophenolato species $[M(-EC_6H_4\text{-}o\text{-}NH-)_2]^-$ (E = Te, Se, S). Specifically, the synthesis and structures of the square planar *trans*-$[Ni(-SeC_6H_4\text{-}o\text{-}NH-)_2]^-$ (**1**) and *cis*-$[Ni(-TeC_6H_4\text{-}o\text{-}NH-)_2]^-$ (**2**) are described. In order to identify the respective oxidation level unambiguously, the oxidation levels of the Ni ion and ligands will be investigated by crystal structural data, electron spin resonance, UV−vis absorption, magnetochemistry, and X-ray absorption spectroscopy of Ni K- and $L_{III, II}$-edges.

Results and Discussion

Synthesis. When a THF solution of 2-aminophenyl diselenide (0.5 mmol, 0.172 g) and $[PPN][Ni^{II}(CO)(SePh)_3]$ (0.5 mmol, 0.545 g)[10] is stirred under N_2, a rapid reaction ensues over the course of 5 min at ambient temperature to give, by what may be described as a reductive elimination/oxidative addition, an extremely air-sensitive intermediate $[Ni(CO)(SePh)(-SeC_6H_4NH_2-)_2]^-$ (Scheme 3a). The IR spectrum (ν_{CO} (THF): 2010 cm^{-1}) of such species did match those of $[Ni(CO)(SPh)_n(SePh)_{3-n}]^-$ (n = 0, 1, 2) complexes as previously established (by IR and X-ray diffraction).[10]

The dark green Se,N-chelated *trans*-$[PPN][Ni(-SeC_6H_4\text{-}o\text{-}NH-)_2]$ (**1**) (Scheme 3b) was isolated as a solid from THF−hexane (0.422 g, 90%) after stirring the solution under

(5) Lee, C.-M.; Lin, G.-Y.; Lee, C.-K.; Hu, C.-H.; Lee, G.-H.; Peng, S.-M.; Liaw, W.-F. *J. Chem. Soc., Dalton Trans.* **1999**, 2393.
(6) (a) Pierpont, C. G.; Buchanan, R. M. *Coord. Chem. Rev.* **1981**, *38*, 45. (b) Attia, A. S.; Pierpont, C. G. *Inorg. Chem.* **1995**, *34*, 1172.
(7) Lim, B. S.; Fomitchev, D. V.; Holm, R. H. *Inorg. Chem.* **2001**, *40*, 4257.
(8) Sellmann, D.; Geck, M.; Knoch, F.; Ritter, G.; Dengler, J. *J. Am. Chem. Soc.* **1991**, *113*, 3819.
(9) (a) Herebian, D.; Bothe, E.; Bill, E.; Weyhermuller, T.; Wieghardt, K. *J. Am. Chem. Soc.* **2001**, *123*, 10012. (b) Chaudhuri, P.; Verani, C. N.; Bill, E.; Bothe, E.; Weyhermuller, T.; Wieghardt, K. *J. Am. Chem. Soc.* **2001**, *123*, 2213. (c) Sun, X.; Chun, H.; Hildenbrand, K.; Bothe, E.; Weyhermuller, T.; Neese, F.; Wieghardt, K. *Inorg. Chem.* **2002**, *41*, 4295.
(10) (a) Liaw, W.-F.; Horng, Y.-C.; Ou, D.-S.; Ching, C.-Y.; Lee, G.-H.; Peng, S.-M. *J. Am. Chem. Soc.* **1997**, *119*, 9299. (b) Liaw, W.-F.; Chen, C.-H.; Lee, C.-M.; Lee, G.-H.; Peng, S.-M. *J. Chem. Soc., Dalton Trans.* **2001**, 138.

air overnight in THF at room temperature. A reasonable reaction sequence accounting for the formation of complex **1** is shown in Scheme 3a,b. Upon contact with air/O_2, the brown reaction mixture immediately turns to dark green in THF. The IR ν(N−H) spectrum (3352 br cm^{-1} (CH_2Cl_2)) indicated the formation of complex **1** accompanied by byproducts of H_2O and diphenyl diselenide identified by ^{1}H NMR.[10] In this oxidative reaction, the oxidation process is best assigned to the yield of diphenyl diselenide from terminal selenolate ligand via radical (•[SePh]) recombination, the subsequent deprotonation of amine proton of the intermediate [Ni(CO)(SePh)(−SeC_6H_4-*o*-NH−)$_2$]$^-$ leading to the formation of H_2O, and, presumably, the concomitant oxidation of the Ni(II) yielding Ni(III) resulting in the displacement of the carbonyl ligand (to our knowledge, no Ni(III)−CO complex was ever observed and reported).[10] The ^{1}H NMR spectra of complex **1** at 298 K do not display any observable signals for the phenyl groups, indicating complex **1** is paramagnetic (either a Ni(III) or a Ni(II)−(π-radical ligand)) at ambient temperature.

Similarly, the reductive elimination/oxidative addition was also displayed by the reaction of complex [PPN][Ni^{II}(CO)(SePh)$_3$] and 2-aminophenyl ditelluride. When a mixed-solvent THF−CH_3CN−CH_2Cl_2 solution of [PPN][Ni^{II}(CO)(SePh)$_3$] was treated with 1 equiv of 2-aminophenyl ditelluride and 2 equiv of triethylamine, an immediate change in color of the solution from dark red-brown to dark green-brown was observed. After extended periods of stirring in the presence of air in CH_3CN−CH_2Cl_2 at room temperature for 1 h, the reaction mixture finally led to the isolation of dark brown compound *cis*-[PPN][Ni(−TeC_6H_4-*o*-NH−)$_2$] (**2**) (Scheme 3a,b). In addition to the X-ray analysis and the UV−vis spectrum, the lower ν(N−H) (3333, 3327 cm^{-1}) compared to that of complex **1** (3352 br cm^{-1}) also supports the formation of complex **2**. Crystals suitable for X-ray diffraction were obtained by diffusion of hexane into its CH_2Cl_2 solution. It can be concluded that replacement of *o*-amidoselenophenolato with the *o*-amidotellurophenolato ligand in complex **1** has a significant effect on its thermal stability and sensitivity toward O_2. The ^{1}H NMR spectra of complex **2** at 298 K also indicate the paramagnetic property.

Treatment of 1 equiv of complex **1** with 2 equiv of 2-aminophenylthiol/1,2-benzenedithiol in THF led to the formation of the known *trans*-[PPN][Ni(−SC_6H_4-*o*-NH−)$_2$] (**3**) and [PPN][Ni(−SC_6H_4-*o*-S−)$_2$] (**4**), respectively (Scheme 3c−e),[11] although the π-bonding ability of bidentate [−SeC_6H_4-*o*-NH−]$^{2-}$ is stronger than that of [−SC_6H_4-*o*-NH−]$^{2-}$/[−SC_6H_4-*o*-S−]$^{2-}$ ligands. It is known that any π-bonding containing an amido group is a more effective donor than the one without an amido group.[1,4] Presumably, the direction of reaction we have observed for the π-bonding ligand metathesis reactions must depend on the formation (stability) of the intermediate [Ni(−SeC_6H_4-*o*-NH_2)$_2$(−SC_6H_4-*o*-EH−)$_2$]$^-$ (E = S, NH) (Scheme 3c), as observed previously.[1] In a similar fashion, reaction of complex **3** with 1,2-benzenedithiol led to the formation of the known complex **4** which is identified by UV and X-ray diffraction (Scheme 3f).[11b]

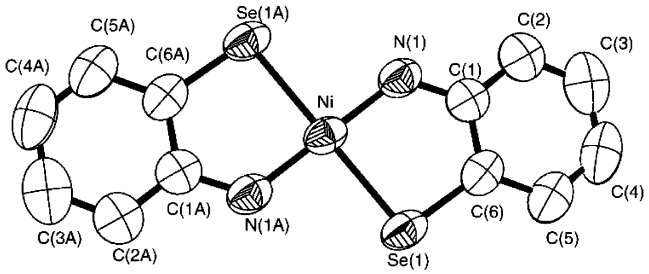

Figure 1. ORTEP drawing and labeling scheme of *trans*-[Ni(−SeC_6H_4-*o*-NH−)$_2$]$^-$. The ellipsoid is at 50% probability.

The electronic structures of complexes **1** and **2** are quite similar since both compounds exhibit an intense absorption at 936 and 942 nm, respectively, with extinction coefficient ϵ > 10000 L mol^{-1} cm^{-1}, but no absorption bands around 600 nm ($\pi \rightarrow \pi^*$ charge-transfer band) and 730−840 nm (ligand-to-ligand charge-transfer band) were detected.[9] As suggested by Wieghardt and co-workers,[9] this result indicates that complexes **1** and **2** contain at least one *o*-iminochalcogenobenzosemiquinonato(1−) π-radical ligand. Obviously, according to the UV−vis spectra, we cannot assign complexes **1** and **2** exactly as a [Ni^{III}(*o*-amidoselenophenolato(2−))$_2$]$^-$ or a [Ni^{III}(*o*-amidotellurophenolato(2−))$_2$]$^-$. If the complex contains two *o*-amidochalcogenophenolato(2−) ligands, it normally does not exhibit an absorption band at longer than 400 nm with intensity greater than 500 L mol^{-1} cm^{-1}.[9] The CV of complex **1** measured in CH_3CN with 0.1 M [*n*-Bu_4N][PF_6] as supporting electrolyte (scan rate 250 mV/s) reveals three pseudoreversible oxidation−reduction potentials at −0.44, −1.22, and −1.43 V ($E_{1/2}$) (vs Ag/$AgClO_4$).

Structure. The molecular structure of *trans*-[Ni(−SeC_6H_4-*o*-NH−)$_2$]$^-$ (**1**) is depicted in Figure 1; selected bond distances and angles are summarized in Table 1. Complex **1** possesses a crystallographically imposed center of inversion symmetry. The geometry around the Ni atom is square planar with a *trans* configuration of the two *o*-amidoselenophenolato ligands in the solid state. Complex **1** exhibits a shorter Ni−Se distance (2.2949(3) Å) than those reported in tetrahedral [Ni(SePh)$_4$]$^{2-}$ (Ni^{II}−Se_{av} = 2.401(3) Å)[12] and [Ni(CO)(SePh)$_3$]$^-$ (average Ni^{II}−Se = 2.317(2) Å)[10] but a longer distance than those observed for [$(C_4H_9)_4N$][Ni(−SeC_6H_4Se−)$_2$] (average Ni−Se = 2.259(9) Å)[13] and [Ni(Se$(CH_2)_2$N(Me)$(CH_2)_2$Se)]$_2$ (average Ni^{II}−Se = 2.255(9) Å, excluding the bridge Se ones).[14] The C−C bond lengths of phenyl rings range from 1.373(5) to 1.415(4) Å in complex **1**.[9]

An ORTEP plot of complex **2** is displayed in Figure 2. The selected bond distances and angles are listed in

(11) (a) Liaw, M.-C.; Lee, G.-H.; Peng, S.-M. *Bull Inst. Chem., Acad. Sin.* **1993**, *40*, 23. (b) Ceasar, G. P.; Gray, H. B. *J. Am. Chem. Soc.* **1969**, *91*, 191.

(12) Goldman, C. M.; Olmstead, M. M.; Mascharak, P. K. *Inorg. Chem.* **1996**, *35*, 2752.

(13) Sandman, D. J.; Allen, G. W.; Acampora, L. A.; Stark, J. C.; Jansen, S.; Jones, M. T.; Ashwell, G. J.; Foxman, B. M. *Inorg. Chem.* **1987**, *26*, 1664.

(14) Choudhury, S. B.; Pressler, M. A.; Mirza, S. A.; Day, R. O.; Maroney, M. J. *Inorg. Chem.* **1994**, *33*, 4831.

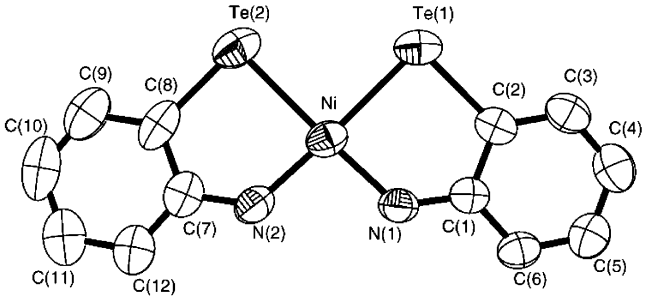

Figure 2. ORTEP drawing and labeling scheme of *cis*-[Ni(−TeC_6H_4-*o*-NH−)$_2$]$^-$. The ellipsoid is as in Figure 1.

Table 1. Selected Bond Distances (Å) and Angles (deg) of Complexes **1** and **2**

		Complex **1**	
Ni−N(1)	1.814(3)	Ni−Se(1)	2.2949(3)
C(1)−N(1)	1.373(4)	Se(1)−C(6)	1.877(3)
C(1)−C(2)	1.415(4)	C(1)−C(6)	1.403(4)
C(2)−C(3)	1.378(4)	C(3)−C(4)	1.373(5)
C(4)−C(5)	1.376(4)	C(5)−C(6)	1.391(4)
N(1)−Ni−Se(1)	88.24(8)	N(1)−C(1)−C(2)	124.4(4)
N(1)−Ni−Se(1A)	91.76(8)	C(6)−Se(1)−Ni	94.04(12)
C(1)−N(1)−Ni	124.8(2)	N(1)−C(1)−C(6)	117.4(4)
		Complex **2**	
Ni−N(2)	1.852(4)	Ni−N(1)	1.859(3)
Ni−Te(1)	2.4441(6)	Ni−Te(2)	2.4450(7)
Te(1)−C(2)	2.100(4)	Te(2)−C(8)	2.080(5)
C(1)−N(1)	1.366(5)	C(7)−N(2)	1.357(5)
C(1)−C(2)	1.412(6)	C(1)−C(6)	1.412(6)
C(2)−C(3)	1.389(6)	C(3)−C(4)	1.371(6)
C(4)−C(5)	1.377(7)	C(5)−C(6)	1.372(6)
C(7)−C(8)	1.404(6)	C(7)−C(12)	1.410(7)
C(8)−C(9)	1.400(6)	C(9)−C(10)	1.363(8)
C(10)−C(11)	1.394(8)	C(11)−C(12)	1.357(7)
N(2)−Ni−N(1)	94.9(2)	Te(2)−Ni−Te(1)	89.92(2)
N(2)−Ni−Te(2)	87.59(14)	N(1)−Ni−Te(2)	174.30(11)
N(2)−Ni−Te(1)	175.74(11)	N(1)−Ni−Te(1)	87.85(11)
C(2)−Te(1)−Ni	90.00(13)	C(1)−N(1)−Ni	129.2(3)
N(1)−C(1)−C(2)	118.6(4)	C(3)−C(2)−Te(1)	125.0(4)

Table 1. Nickel is best described as in a distorted square planar coordination surrounded by two *o*-amidotellurophenolato ligands with the bite angles of 87.85(11)° and 87.59(11)°, respectively. Two tellurium atoms are disposed in a *cis* arrangement while *trans* to the nitrogen atoms. The intramolecular Te···Te contact distance of 3.455 Å is considerably longer than that of a typical single bond length of 2.7574(3) Å in H_2N-*o*-C_6H_4Te−TeC_6H_4-*o*-NH_2[15] but comparable to the Te···Te contact distance of 3.495 Å in a Cs_2Te_5 complex[16] which is considered to be a significant interchain interaction. This intramolecular Te···Te contact interaction may contribute to the stabilization of complex **2** with a *cis* configuration having 89.92(3)° for Te(2)−Ni−Te(1) and 94.9(2)° for N(2)−Ni−N(1) , respectively. In contrast, the structure of $[Pd(L^{AP})_2][HNEt_3][CH_3CO_2]$ ($[L^{AP}]^{1-}$ = *o*-aminothiophenolate) adopts a *cis* configuration deriving from both *cis* coordinated NH_2 groups of *cis*-$[Pd(L^{AP})_2]$ binding weakly to two oxygen atoms of an acetate $[CH_3CO_2]^-$.[9] The Ni−Te(1) and Ni−Te(2) bond lengths of

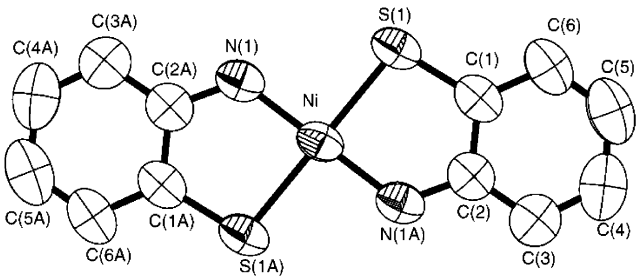

Figure 3. ORTEP drawing and labeling scheme of *trans*-[Ni(−SC_6H_4-*o*-NH-)$_2$]$^-$. The ellipsoid is as in Figure 1.

Table 2. Selected Bond Distances (Å) and Angles (deg) of Complex **3**

Ni−N(1)	1.8135(19)	Ni−S(1)	2.1713(6)
C(2)−N(1A)	1.369(3)	S(1)−C(1)	1.735(2)
C(1)−C(2)	1.401(3)	C(1)−C(6)	1.391(3)
C(2)−C(3)	1.410(3)	C(3)−C(4)	1.372(3)
C(4)−C(5)	1.376(4)	C(5)−C(6)	1.378(4)
N(1)−Ni−S(1)	92.14(6)	C(1)−S(1)−Ni	98.03(9)
N(1)−Ni−S(1A)	87.86(6)	N(1A)−C(2)−C(3)	125.1(2)
C(2A)−N(1)−Ni	122.22(17)		

Table 3. Comparisons of the Selected Bond Distances (Å) and Angles (deg) for Complexes **1**, **2**, and **3**

	E = S (**3**)	E = Se (**1**)	E = Te (**2**)
Ni−N	1.8135(19)	1.814(3)	1.859(3), 1.852(4)
Ni-E	2.1713(6)	2.2949(3)	2.4441(6), 2.4450(7)
N−C	1.369(3)	1.373(4)	1.366(5), 1.357(5)
E−C	1.735(2)	1.877(3)	2.100(4), 2.080(5)
N−Ni−N			94.9(2)
E−Ni−E			89.92(2)
N−Ni−E	87.86(6)	88.24(8)	87.85(11), 87.59(11)

2.4450(7) and 2.4441(6) Å in complex **2** are shorter than the Ni(II)−Te bond distance of 2.4804(6) Å in the complex CpNi(TePh)(PPh_3).[17] Alternation in C−C bond lengths of phenyl rings, spanning the range from 1.357(7) to 1.412(6) Å, are observed.[9]

The structure of *trans*-[Ni(−SC_6H_4-*o*-NH−)$_2$]$^-$ (**3**) is shown in Figure 3. The selected bond distances and angles are given in Table 2.[11] Further appropriate comparisons lie in the N−C and Ni−N parameters (Table 3); the N−C bond distances (1.369(3) Å for complex **3**, 1.373(4) Å for **1** and 1.362(5) Å (average) for **2**) are not disturbed by the change of donor sets (S, Se, Te) in complexes **1**, **2**, and **3**. The variation of Ni−E bond lengths (E = S, Se, Te; 2.1713(6) Å for **3**, 2.2949(3) Å for **1** and 2.4450(7) Å for **2**) gives **3** < **1** < **2** (Table 3). However, the N−Ni−E bond angles (E = Se, Te, S) of these three complexes are essentially the same (88.24(8)°, 87.72(11)°, and 87.86(6)°) (Table 3). It is worth noticing that the C(1)−N(1) distance of 1.373(4) Å in complex **1** and C(1)−N(1)/C(7)−N(2) distances of 1.367-(7)/1.377(7) Å in complex **2**, respectively, are slightly longer than those observed for the transition-metal *o*-iminothionebenzosemiquinonato(1−) π-radical complexes (average C−N bond lengths of 1.356 Å) but significantly shorter than those observed for the transition-metal *o*-amidothiophenolato-(2−) complexes (average C−N bond lengths of 1.413 Å).[9]

Obviously, the UV−vis spectrum and X-ray structural data lend support to the notion, developed by Wieghardt and

(15) Liaw, W.-F.; Ou, D.-S.; Li, Y.-S.; Lee, W.-Z.; Chuang, C.-Y.; Lee, Y.-P.; Lee, G.-H.; Peng, S.-M. *Inorg. Chem.* **1995**, *34*, 3747.
(16) Burns, R. C.; Gillespie, R. J.; Luk, W. C.; Slim, D. R. *Inorg. Chem.* **1979**, *18*, 3086.
(17) Hsieh, C.-K.; Lo, F.-C.; Lee, G.-H.; Peng, S.-M.; Liaw, W.-F. *J. Chin. Chem. Soc. (Taipei)* **2000**, *47*, 103.

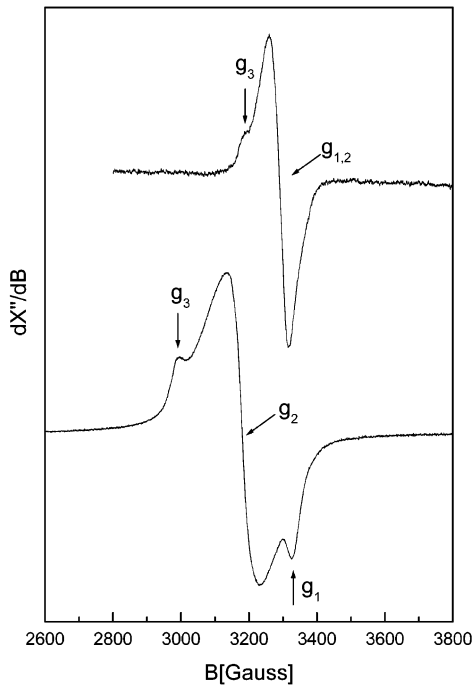

Figure 4. EPR spectra of complex **1** (top) and **2** (bottom) frozen in CH_2Cl_2 (4.2 K), respectively.

Scheme 4

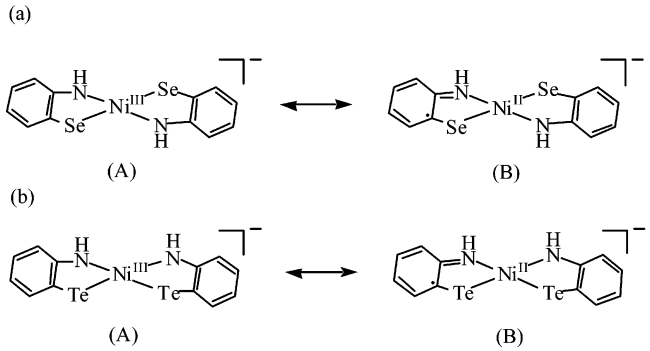

co-workers,[9] that complexes **1** and **2** contain delocalized oxidation levels of the nickel ion and ligands, namely a resonance hybrid of **A** (a paramagnetic Ni^{III} (d^7) central ion with two dianionic *o*-amidochalcogenophenolato(2−)) and **B** (a diamagnetic Ni^{II} (d^8) central ion with *o*-amidochalcogenophenolato(2−) as well as *o*-iminochalcogenobenzosemiquinonato(1−) π-radical ligands), as shown in Scheme 4a,b.

EPR Spectroscopy. The ground state electronic structures of complexes **1** and **2** have also been investigated by the variable temperature (4−300 K) EPR measurements. EPR spectra of complex **1** (top) and complex **2** (bottom) frozen in CH_2Cl_2 at 4.2 K are shown in Figure 4. The EPR signal remains unchanged from room temperature down to 4.2 K. The unresolved EPR spectrum of complex **1** exhibits an observable but rather small *g*-tensor anisotropy, with all *g* values greater than 2.0023. The slight rhombic distortion in complex **1** is not obvious enough to be discerned from the experimental EPR spectra directly and is obtained by computer simulations with simulated principal *g* values at $g_1 = 2.036$, $g_2 = 2.062$, and $g_3 = 2.120$. Complex **2** exhibits a rhombic EPR spectrum and larger principal *g* values at $g_1 = 2.021$, $g_2 = 2.119$, and $g_3 = 2.250$ due to larger spin−orbit coupling of the heavier chalcogen atom, Te.[9c]

Three possible spin configurations exist for these monoanionic complexes **1** and **2**, namely, L*−Ni(I)−L*, L−Ni(III)−L, and L−Ni(II)−L*; here, the L* denotes the *o*-imino-(seleno/telluro)benzosemiquinonato ligand with a radical residing on the ligand (Scheme 2b), and L denotes the amido-(seleno/telluro)phenolato ligand(2−) (Scheme 2a). According to the X-ray absorption spectroscopy and magnetic measurement of complexes **1** and **2**, it seems rather unlikely to support the presence of a Ni(I) oxidation state, which will be discussed in the following section. Therefore, the possibility of the three-spin coupled L*−Ni(I)−L* spin configuration ($^1/_2$, 1) is ruled out.[9,18] It leaves ($^1/_2$, 0) and ($^1/_2$, $^1/_2$) as the ground state of the L−Ni(III)−L and L−Ni(II)−L* spin configurations, respectively; here the spin states (S_t, S^*) are labeled by their total spin $S_t = S_{ligand1} + S_{Ni} + S_{ligand2}$ and a subspin of the ligand $S^* = S_{ligand1} + S_{ligand2}$.[19]

For the L−Ni(III)−L configuration with an unpaired electron localized at the metal ion, the EPR *g* tensor generally exhibits considerable anisotropies and a large deviation from the free electron *g* value as described in detail by Holm et al.[20,21] and Lovecchio et al.,[22] respectively (Table 4). Thus, the observed small *g* anisotropy with g_{av}=2.073 for complex **1** does not support the single metal centered (Ni(III)) unpaired electron. However, such a conclusion is not so straightforward for complex **2**. Although the *g* anisotropy of **2** is much bigger than that of **1**, the anisotropy of **2** could be due to the large spin−orbital coupling of Te through M−L π-interaction.

The ligand radical stabilized by the Ni(II) configuration, L−Ni(II)−L*, produces a typical radical EPR signal with an isotropic *g* value closed to 2.00 (Table 4). Apparently, the EPR spectrum of complex **1** is indicative of the ligand radical characters but with a contribution of the Ni(III) d orbital leading to the observed small *g* anisotropy.

Since none of the configurations discussed here could, alone, fully account for the observed EPR spectra, we suggest that the spin configuration is better described as delocalized systems described for the low spin Ni(III) d^7 square planar complex $[Ni(S_2C_2(CN)_2)_2]^-$, for which a $3d_{yz}/d_{xz}$ ($d_{yz}/d_{xz}-p_\pi$) ground state and spin delocalization were deduced.[23−25] The delocalization of unpaired spin density was further

(18) Wang, H.; Ralston, C. Y.; Patil, D. S.; Jones, R. M.; Gu, W.; Verhagen, M.; Adams, M.; Ge, P.; Riordan, C.; Marganian, C. A.; Mascharak, P.; Kovacs, J.; Miller, C. G.; Collins, T. J.; Brooker, S.; Croucher, P. D.; Wang, K.; Stiefel, E. I.; Cramer, S. P. *J. Am. Chem. Soc*. **2000**, *112*, 10544.
(19) Kambe, K. *J. Phys. Soc. Jpn*. **1950**, *5*, 48.
(20) Forbes, C. E.; Gold, A.; Holm, R. H. *Inorg. Chem*. **1971**, *10*, 2479.
(21) Holm, R. H.; Balch, A. L.; Davison, A.; Maki, A. H.; Berry, T. E. *J. Am. Chem. Soc*. **1967**, *89*, 2866.
(22) Lovecchio, F. V.; Gore, E. S.; Busch, D. H. *J. Am. Chem. Soc*. **1974**, *96*, 3109.
(23) Maki, A. H.; Edelstein, N.; Davison, A.; Holm, R. H. *J. Am. Chem. Soc*. **1964**, *86*, 4580.
(24) Davison, A.; Edelstein, N.; Holm, R. H.; Maki, A. H. *Inorg. Chem*. **1964**, *3*, 814.
(25) (a) Lim, B. S.; Fomitchev, D. V.; Holm, R. H. *Inorg. Chem*. **2001**, *40*, 4257. (b) Stein, M.; van Lenthe, E.; Baerends, E. J.; Lubitz, W. *J. Phys. Chem. A* **2001**, *105*, 416.

Table 4. Electronic (*g* Tensor) Parameters for Square Planar Ni Complexes

complex	g_1	g_2	g_3	g_{iso}	oxidation state characterization
1	2.036	2.062	2.120		
2	2.021	2.119	2.250		
		Ligand Radical with Metal d Characters (Delocalized System)			
$[1a/1b]^-$	2.0282	2.0055	2.1147		ligand ladical + Ni(I) $d_{x^2-y^2}$ character[9]
$[Ni(S(NH)C_6H_4)_2]^-$	2.028	2.005	2.126		ligand radical + metal character[21]
$[NiS_4C_4(CN)_4]^-$	2.14	2.04	1.99		delocalized spin with Ni(III) d_{yz} character[23−25]
$[Ni(S_2C_2Me_2)_2]^-$	2.118	2.041	2.000		delocalized spin with Ni(III) d_{yz} character[23−25]
		Ligand Radical			
$[NiMe_2[14]1,3\text{-dieneN}_4]^-$				2.004	ligand radical[22]
$[NiMe_6[14]1,3,7,11\text{-tetraeneN}_4]^-$				2.003	ligand radical[22]
$[1a/1b]^+$	1.9970	1.9901	2.0172	2.0014	ligand radical[9]
		Metal Centered Oxidation State			
$[NiMe_6[14]1,4,8,11\text{-tetraeneN}_4]^-$	2.053	2.053	2.195		Ni(I)[22]
$[NiMe_6[14]4,11\text{-dieneN}_4]^-$	2.055	2.055	2.226		Ni(I)[22]
$[NiMe_6[14]1,4,8,11\text{-tetraeneN}_4]^+$	2.186	2.186	2.018		Ni(III)[22]
$[NiMe_6[14]4,11\text{-dieneN}_4]^+$	2.199	2.199	2.024		Ni(III)[22]
$[NiMe_6[14]1,3,7,11\text{-tetraeneN}_4]^+$	2.180	2.180	2.016		Ni(III)[22]

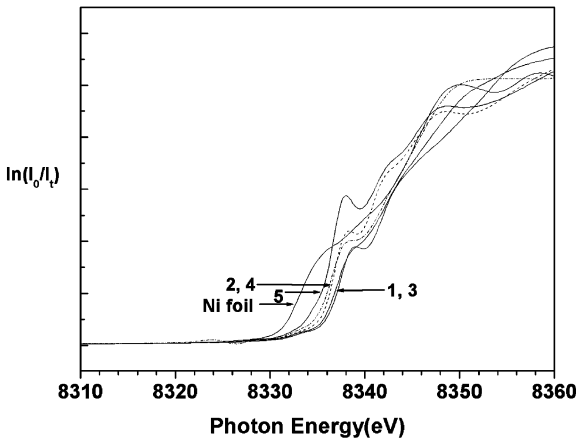

Figure 5. X-ray absorption near edge spectroscopy (XANES) of Ni: K-edge spectra of Ni foil and Ni complexes **1**, **2**, **3**, **4** [t-Bu_4P][Ni(−SC_6H_4-*o*-S−)$_2$], and **5** $Ni(S_2CNBu_2)_2$.

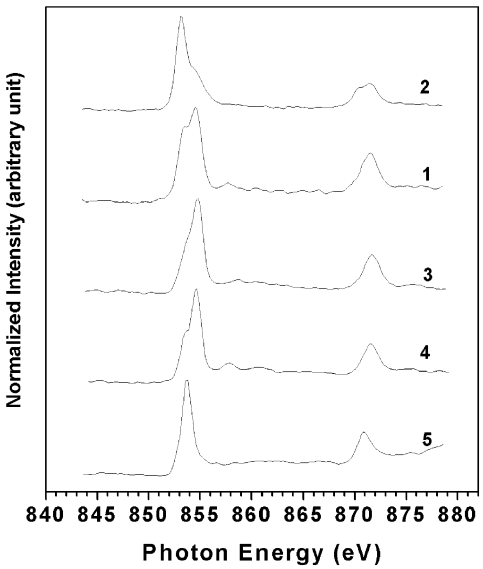

Figure 6. X-ray absorption spectroscopy of Ni $L_{III,\ II}$-edge spectra of some Ni complexes **1**−**5** are as in Figure 5.

characterized by ENDOR[26] and ESEEM[26] of ^{13}C and $^{14,15}N$ isotopomers of such a complex. The fact that the unpaired electron is delocalized onto the ligands supports the observed small anisotropy of the *g* factor and the decreases in *g* values for complex **1**.

X-ray Absorption Spectroscopy. In order to clarify the detailed electronic structure (oxidation state) of the central nickel ion in complexes **1**−**4**, the X-ray absorption measurements were undertaken. The K-edge absorption spectra of complexes **1**−**4** are displayed in Figure 5. A typical Ni(0) of Ni foil and a square planar, low spin, diamagnetic d^8 Ni(II) complex **5,** $Ni(S_2CNBu_2)_2$, are included for references. As shown in Figure 5, the absorption edge E_0 of Ni(II) complex **5** is higher than that of Ni(0). The even higher energy E_0 of **1**−**4** than that of **5** implies a higher oxidation state of Ni in these complexes. Among them, the E_0 values of **1** and **3** are slightly higher than those of **2** and **4**.

The Ni $L_{III,\ II}$-edge absorption spectra of complexes **1**−**4** are depicted in Figure 6 together with that of a typical Ni(II) complex, **5**. The main L_{III} peak at ∼854.5 eV, an indication of Ni(III) oxidation state, was observed with a shoulder at ∼853.5 eV for complexes **1**−**4**, individually. Recently, it was reported that the average centroids of the L_{III} edge of Ni(I), Ni(II, high spin)/Ni(II, low spin), and Ni(III) complexes are at 852.5, 853.4/853.5, and 854.5 eV, respectively.[18,27,28] However, it was also realized that a Ni(III) absorption is often accompanied by the presence of Ni(II) due to the charge transfer (LMCT) mechanism.[29] Apparently, complexes **1**, **3**, and **4** all have the main L_{III} and L_{II} absorption peaks at ∼854.5 and ∼871.5 eV, respectively, which is a

(26) Huyett, J. E.; Choudhury, S. B.; Eichhorn, D. M.; Bryngelson, P. A.; Maroney, M. J.; Hoffman, B. M. *Inorg. Chem.* **1998**, *37*, 1361.

(27) Ralston, C. Y.; Wang, H.; Ragsdale, S. W.; Kumar, M.; Spangler, N. J.; Ludden, P. W.; Gu, W.; Jones, R. M.; Patil, D. S.; Cramer, S. P. *J. Am. Chem. Soc.* **2000**, *122*, 10553.

(28) Wang, H.; Patil, D. S.; Gu, W.; Jacquamet, L.; Friedrich, S.; Funk, T.; Cramer, S. P. *J. Electron Spectrosc. Relat. Phenom.* **2001**, *114*−*116*, 855−863.

(29) De Nadaï, C.; Demourgues, A.; Grannec, J.; de Groot, F. M. F. *Phys. Rev. B* **2001**, *63*, 125123.

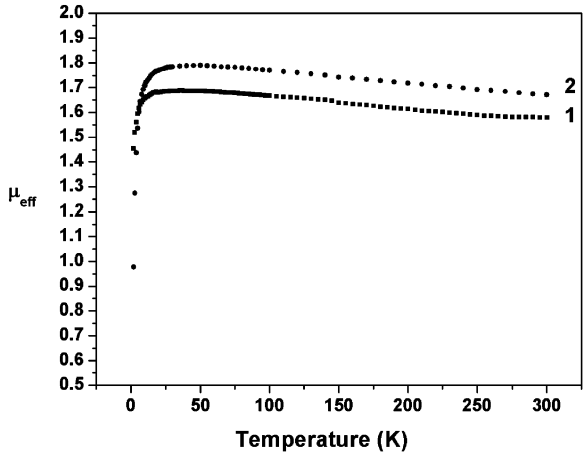

Figure 7. Plots of μ_{eff} vs T for complexes **1** and **2**, respectively.

typical Ni(III). A shoulder peak at this energy is also observed in complex **2**. Taking a closer look of the absorption spectra, an additional absorption peak at ~853.5 eV is observed for all complexes. A plausible interpretation of these spectra is mixed Ni(II) ↔ Ni(III) states existing in all these complexes, where the major component is Ni(III) for **1**, **3**, and **4**. No Ni(I) state is observed between the edges of Ni foil and of **5**. The L_{III}-edge absorption spectrum of complex **1** is similar to that of K_3NiF_6,[18] and the simulated spectra using a ligand field multiplet calculation on the basis of Ni(III) in D_{4h} symmetry with the charge-transfer effect being taken into account;[18,29,30] i.e., it contains a $3d^7$ and $3d^8\underline{L}$ mixed state where $\underline{L}$ means an electron hole at a ligand site.[29,30] In fact, this is consistent with what was found in the EPR measurement, where a L−Ni(III)−L and a L−Ni(II)−L* (or L*−Ni(II)−L) with a spin state of ($^1/_2$, 0) and ($^1/_2$, $^1/_2$) as a ground state, respectively.

The magnetic measurements of complexes **1** and **2** are shown in Figure 7. It is roughly in accord with one net unpaired electron of $\mu_{eff} \sim 1.6\mu_B$ and $\sim 1.7\mu_B$ for complexes **1** and **2**, respectively; however, the temperature dependence is very small though detectable. It is unlikely to be described as three unpaired electrons coupled together to yield a net one unpaired electron, i.e., a ($^1/_2$, 1) state which supposedly will give a large temperature dependence. Therefore, a mixed spin state of ($^1/_2$, 0) and ($^1/_2$, $^1/_2$) is ascribed for such a magnetic measurement.

DFT Computation. In order to compare the SOMOs[25,26] of these complexes with those of the $[Ni(S_2C_2Me_2)_2]^-$ and $[Ni(S_2C_2(CN)_2)_2]^-$ complexes, a density functional theory based on MO calculation at unrestricted ZORA scalar relativistic BP/TZ2P level was performed. The derived SOMOs of complexes **1** and **2** are depicted in Figure 8a,b, respectively, which shows an antibonding π-character between the $3d_{xz}$ orbital of the nickel ion and the π*-orbital of the ligand in both complexes. The outcome is consistent with the SOMOs of $[Ni(S_2C_2(CN)_2)_2]^-$ and $[Ni(S_2C_2Me_2)_2]^-$ which reconfirms the L−Ni(III)−L and L−Ni(II)−L* configuration and in accord with EPR measurements and X-ray absorption spectra.

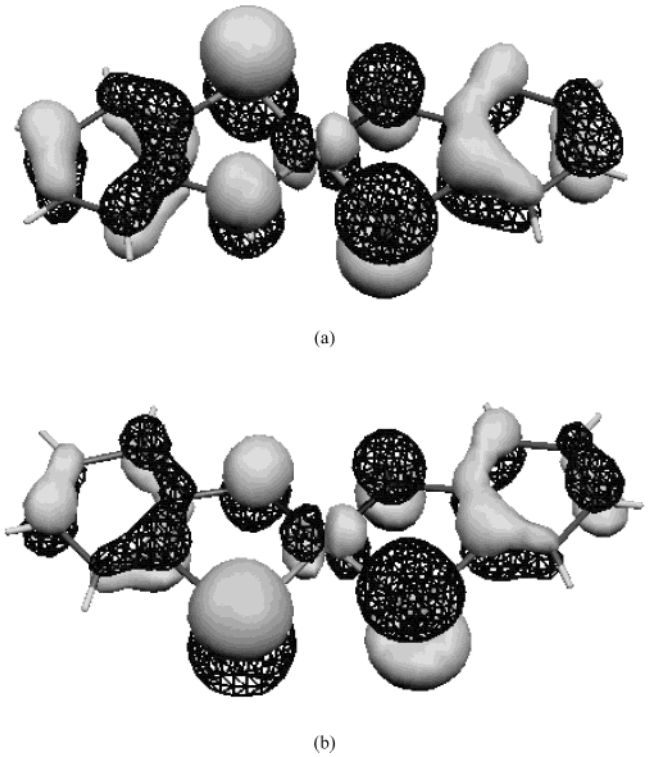

Figure 8. SOMO of (a) complex **1** and (b) complex **2**. Solid and mesh surfaces are of opposite sign.

As seen in Figure 8a,b, the unpaired electron is indeed delocalized between the Ni and the ligands. The ligand π*-orbital is mainly contributed by the following orbitals: $4p_z$ of selenium, $5p_z$ of tellurium, and $2p_z$ of nitrogen. This MO can be realized as metal-to-ligand back-bonding, and thus, the ligand is serving as a π-acceptor. Mülliken population analysis gave the atomic spin density of each selenium (tellurium), nitrogen, and nickel atom as 0.083 (0.144), 0.138 (0.104), and 0.345 (0.339), respectively. The residual spin density of ~0.21 (~0.16) is dissipated equally onto the two phenyl rings. The total unpaired spin density of ~0.78 and ~0.75 of the core of complexes **1** and **2**, respectively, is comparable with that of the $[NiS_4]$ core of $[Ni(S_2C_2(CN)_2)_2]^-$ (~0.85 and ~0.75 derived from ENDOR and DFT,[26] respectively) and of $[Ni(S_2C_2Me_2)_2]^-$ (~0.79 derived from DFT[25]).

Summary. Complex $[Ni(CO)(SePh)_3]^-$ provides a convenient preparative entry to the complexes *trans*-$[Ni(-SeC_6H_4\text{-}o\text{-}NH-)_2]^-$ (**1**), *cis*-$[Ni(-TeC_6H_4\text{-}o\text{-}NH-)_2]^-$ (**2**), *trans*-$[Ni(-SC_6H_4\text{-}o\text{-}NH-)_2]^-$ (**3**), and $[Ni(-SC_6H_4\text{-}o\text{-}S-)_2]^-$ (**4**). Square planar structures of complexes **1**−**3** have been characterized by X-ray analysis. The anisotropy in g values of these complexes from EPR measurement as well as the magnetic measurement is consistent with the spin located either at the Ni site or at one of the ligand sites, i.e., L−Ni(III)−L or L−Ni(II)−L* with probable ($^1/_2$, 0) or ($^1/_2$, $^1/_2$) as the ground state. The spin exchange between Ni and L could be accomplished through the Ni−L π bond, namely $p_z-d_{xz}/d_{yz}-p_z$ molecular orbitals as realized by DFT calculation. Ni L_{III}-peaks at ~853.5 and ~854.5 eV for complexes **1**−**4** also indicate the existence of the Ni(II) and Ni(III) valence state. On the basis of the X-ray structural data,

(30) Hu, Z.; Kaindl, G..; Warda, S. A.; Reinen, D.; de Groot, F. M. F.; Müller, B. G. *Chem. Phys.* **1998**, *232*, 63.

magnetic measurements, and UV−vis, EPR, and X-ray K- and L-edge absorption spectroscopy, a delocalized oxidation level of the nickel ion and ligands is proposed for complexes **1**−**4**, as shown in Scheme 4. We noticed that the monoanionic complex $[Pt(L^{ISQ})_2]^-$ (L^{ISQ} = *o*-iminobenzosemiquinonate(1−)), reported by Wieghardt and co-workers very recently,[9c] is best described as a delocalized mixed-valence system where the unpaired electron is mainly located on the ligands and the delocalized SOMO acquires some metal d character by mixing with the d orbital of the Pt (the observed *g* anisotropy). This elucidation may further explain the observations of this study in complexes **1**−**4**, especially complex **2** with the suspected large spin−orbit coupling of the Te through M−L π-interaction.

Experimental Section

Manipulations, reactions, and transfers of samples were conducted under nitrogen according to standard Schlenk techniques or in a glovebox (argon gas). Solvents were distilled under nitrogen from appropriate drying agents (diethyl ether from CaH_2, acetonitrile from $CaH_2-P_2O_5$, methylene chloride from P_2O_5, hexane and tetrahydrofuran (THF) from sodium−benzophenone) and stored in dried, N_2-filled flasks over 4 Å molecular sieves. Nitrogen was purged through these solvents before use. Solvent was transferred to a reaction vessel via a stainless steel cannula under positive pressure of N_2. The reagents iron pentacarbonyl, cyclopentadienylnickel carbonyl dimer, bis(triphenylphosphoranylidene)ammonium chloride (Lancaster/Aldrich), triethylamine (TCI), 2-aminophenylthiol, diphenyl diselenide, 2-aminophenyl diselenide (Arcos), and 1,2-benzenedithiol (Fluka) were used as received. The compound 2-aminophenyl ditelluride was synthesized and characterized by published procedures.[31] Infrared spectra of the ν(NH) stretching frequencies were recorded on a Bio-Rad model FTS-185 spectrophotometer with sealed solution cells (0.1 mm) and KBr windows. UV−vis spectra were recorded on a Hewlett-Packard 71 spectrophotometer. Cyclic voltammograms were obtained from 2 mM analyte concentration in CH_3CN using 0.1 M [*n*-Bu_4N][PF_6] as supporting electrolyte (scan rate 250 mV/s). Analyses of carbon, hydrogen, and nitrogen were obtained with a CHN analyzer (Heraeus).

Preparation of *trans*-[PPN][Ni(−SeC$_6$H$_4$-*o*-NH−)$_2$] (1). The compounds [PPN][Ni(CO)(SePh)$_3$] (0.5 mmol, 0.545 g) and 2-aminophenyl diselenide (0.5 mmol, 0.172 g) were dissolved in 5 mL of THF and stirred at ambient temperature overnight. Upon contact with air, the color of the reaction mixture immediately turned from dark brown to dark green. The solution was then filtered through Celite, and hexane (15 mL) was added to precipitate the dark green solid *trans*-[PPN][Ni(−SeC$_6$H$_4$-*o*-NH−)$_2$] (**1**) (0.422 g, 90%). Diffusion of hexane into a CH_2Cl_2 solution of complex **1** at −15 °C for 4 weeks led to dark green crystals suitable for X-ray crystallography. IR (CH_2Cl_2): 3352 br (ν_{NH}) cm^{-1}. Absorption spectrum (CH_2Cl_2) [λ_{max}, nm (ϵ, M^{-1} cm^{-1})]: 312(21520), 372(8800), 405(6960) (sh), 623(1600), 693(2297), 936(13603). Anal. Calcd for $C_{48}H_{40}NiN_3Se_2P_2$: C, 61.50; H, 4.30; N, 4.48. Found: C, 61.08; H, 4.27; N, 4.26.

Preparation of *cis*-[PPN][Ni(−TeC$_6$H$_4$-*o*-NH−)$_2$] (2). 2-Aminophenyl ditelluride (0.5 mmol, 0.220 g) was added to a THF (10 mL) solution containing 0.545 g (0.5 mmol) of [PPN][Ni(CO)(SePh)$_3$] and stirred at ambient temperature for 1 h. Triethylamine (1 mmol, 139 μL) and $CH_3CN-CH_2Cl_2$ (2 mL + 2 mL) solvent were then added by syringe to the reaction mixture, respectively. Upon contact with air, the color of reaction mixture immediately turned from dark red-brown to dark green-brown. The resulting mixture was filtered through Celite, and then, hexane was added to precipitate the dark brown solid *cis*-[PPN][Ni(−TeC$_6$H$_4$-*o*-NH−)$_2$] (**2**). Recrystallization from saturated CH_2Cl_2 solution of complex **2** with hexane diffusion at ambient temperature gave dark brown crystals (0.285 g, 53%) suitable for X-ray crystallography. IR (CH_2Cl_2): 3333, 3327 (ν_{NH}) cm^{-1}. Absorption spectrum (CH_2Cl_2) [λ_{max}, nm (ϵ, M^{-1} cm^{-1})]: 331(12485), 413(4485), 552(1353), 707(1745), 847(5351), 942(10105). Anal. Calcd for $C_{48}H_{40}NiN_3Te_2P_2$: C, 54.66; H, 4.20; N, 3.98. Found: C, 55.77; H, 4.63; N, 4.31.

Preparation of *trans*-[PPN][Ni(−SC$_6$H$_4$-*o*-NH−)$_2$] (3). 2-Aminophenylthiol (0.5 mmol, 50 μL) was added dropwise by syringe to a solution containing 0.468 g (0.5 mmol) of complex **1** in CH_2Cl_2 (5 mL). The reaction solution was then stirred at ambient temperature overnight. The solution was filtered through Celite, and hexane (15 mL) was added to precipitate the dark green solid *trans*-[PPN][Ni(−SC$_6$H$_4$-*o*-NH−)$_2$] (**3**) (0.262 g, 62%).[11a] Diffusion of hexane into a CH_2Cl_2 solution of complex **3** at −15 °C for 4 weeks yielded dark green crystals suitable for X-ray crystallography. IR (CH_2Cl_2): 3357 (ν_{NH}) cm^{-1}. Absorption spectrum (CH_2Cl_2) [λ_{max}, nm (ϵ, M^{-1} cm^{-1})]: 326(11649), 411(4828), 628(1741), 912(12118) (sh), 945(12573).

Reaction of 1,2-Benzenedithiol and Complex 1. Initially, 1.2-benzenedithiol (0.2 mmol, 24 μL) was added dropwise by syringe to a solution containing 0.187 g (0.2 mmol) of complex **1** in CH_2Cl_2 (5 mL). After the reaction solution was stirred for 1 h at room temperature, hexane was added to precipitate the known dark green solid *trans*-[PPN][Ni(−SC$_6$H$_4$-*o*-S−)$_2$] (**4**).[11b] The stable product **4** was washed twice with CH_2Cl_2−hexane and dried under vacuum. Crystals suitable for X-ray crystallography were grown by vapor diffusion of hexane into a concentrated CH_2Cl_2 solution of **4** at −15 °C. Absorption spectrum (CH_2Cl_2) [λ_{max}, nm (ϵ, M^{-1} cm^{-1})]: 312(17049), 357(7107), 663(1217), 818(5306) (sh), 879(9401).

Crystallography. Crystallographic data of complexes **1**−**3** are summarized in Table 5, and in the Supporting Information. The crystals of **1**−**3** are chunky. The crystals of **1**−**3** chosen for X-ray diffraction studies measured 0.42 × 0.32 × 0.30 mm^3, 0.30 × 0.28 × 0.25 mm^3, and 0.34 × 0.30 × 0.16 mm^3, respectively. Each crystal was mounted on a glass fiber and quickly coated in epoxy

Table 5. Crystal Data of Complexes **1**, **2**, and **3**

	1	**2**	**3**
chem formula	$C_{48}H_{40}N_3P_2Se_2Ni$	$C_{52}H_{50}ON_3P_2Te_2Ni$	$C_{48}H_{40}N_3P_2S_2Ni$
fw	937.40	1108.80	843.60
cryst syst	monoclinic	monoclinic	monoclinic
space group	*C*2/*c*	*P*2$_1$/*n*	*C*2/*c*
λ(Mo Kα), Å	0.7107	0.7107	0.7107
a, Å	18.1779(12)	16.7321(9)	18.2656(12)
b, Å	11.3673(8)	13.0594(7)	11.1299(7)
c, Å	20.4646(14)	22.4392(13)	20.3728(14)
α, deg	90	90	90
β, deg	99.485(2)	96.892(1)	99.713 (1)
γ, deg	90	90	90
V, Å^3	4170.9(5)	4867.8(5)	4082.3(5)
Z	4	4	4
d_{calcd}, g cm^{-3}	1.493	1.513	1.373
μ, mm^{-1}	2.325	1.679	0.695
T, K	293(2)	293(2)	293(2)
R	0.0398[a]	0.0342[a]	0.0334[a]
$R_w(F^2)$	0.0455[b]	0.0759[b]	0.0654[b]
GOF	1.048	1.039	0.829

[a] $R = \sum|(F_o-F_c)|/\sum F_o$. [b] $R_w(F^2) = \{\sum w(F_o^2 - F_c^2)^2/\sum[w(F_o^2)^2]\}^{1/2}$.

(31) Engman, L.; Stern, D.; Cotgreave, I. A.; Andersson, C. M. *J. Am. Chem. Soc.* **1992**, *114*, 9737.

resin. Unit cell parameters were obtained by least-squares refinement. Diffraction measurements for complexes **1**−**3** were carried out on a SMART CCD diffractometer with graphite-monochromated Mo Kα radiation ($\lambda = 0.7107$ Å) and θ between 2.02° and 27.52° for complex **1**, between 1.44° and 27.50° for complex **2**, and between 2.03° and 27.55° for complex **3**. Least-squares refinement of the positional and anisotropic thermal parameters of all non-hydrogen atoms and fixed hydrogen atoms was based on F^2. A SADABS[32] absorption correction was made. The SHELXTL[33] structure refinement program was employed.

X-ray Absorption Measurements. All X-ray absorption experiments were carried out at the Synchrotron Radiation Research Center (SRRC), Hsinchu, Taiwan. Both Ni K-edge and L-edge data were recorded at room temperature. Samples of [PPN][Ni(EC_6H_4-*o*-$NH)_2$] (E = Se, Te, S) are single crystals, and those of [*t*-Bu_4P]-[Ni(SC_6H_4-*o*−$S)_2$] and $Ni^{II}(S_2CNBu_2)_2$ were purchased from TCI. For Ni K-edge measurements, the experiments were performed in transmission mode at the BL-17C X-ray Wiggler beamline with a double crystal Si(111) monochromator. The higher X-ray harmonics were minimized by detuning the double-crystal monochromator to 80% of the maximum. The spectra were scanned from 8.132 to 9.326 keV using a gas-ionization detector. A reference Ni foil is always used simultaneously for the calibration of energy. The ion chambers used to measure the incident (I_0) and transmitted (I) intensities were filled with a mixture of N_2 and He gases and a mixture of N_2 and Ar gases, respectively.

For Ni L-edge measurements, the data were collected at the 6-m high-energy spherical grating monochromator (HSGM) beamline with 40 μm opening slits, corresponding to ∼0.3 eV energy resolution for the Ni L-edge energy range. All samples were ground to powder from single crystals, stuck to conducting tape, and then subjected to an ultrahigh vacuum chamber (10^{-9} Torr). The spectra were recorded in total electron yield mode with a microchannel plate as detector. Each spectrum was calibrated by using the known L_{III}-edge absorption peak at 853.2 eV of NiO.

EPR Measurements. EPR measurements were performed at X-band using a Bruker EMX spectrometer equipped with a Bruker TE102 cavity and a Bruker VT2000 temperature control unit (120−300 K). For liquid helium temperature measurements, an Oxford ESR910 continuous flow cryostat (4−200 K) was used. X-band EPR spectra of complexes **1** and **2** frozen in CH_2Cl_2 were obtained with a microwave power of 2 mW, frequency at 9.468 GHz (Figure 4 (top), complex **1**) and 9.416 GHz (Figure 4 (bottom), complex **2**), and modulation amplitude of 0.1 mT at 100 kHz (temperature = 4.2 K).

Magnetic Measurements. The magnetization data were recorded on a SQUID magnetometer (MPMS7 Quantum Design company) with an external 1.0 T magnetic field in the temperature range from 2−300 K. The magnetic susceptibility of the experimental data was corrected for diamagnetism by the tabulated Pascal's constants.

Computational Details. The spin-unrestricted DFT calculations were carried out using the ADF2002.02[34] package. All electrons were included in the calculation. The zero-order regular approximation (ZORA)[35] Hamiltonian was used to include the relativistic effects referred to as scalar relativistic (SR) effects and spin−orbit (SO) coupling. The local density approximation (LDA) utilized the Vosko−Wilk−Nusair (VWN)[36] functional, and the nonlocal corrections were the Becke exchange[37] and Perdew correlation[38] functionals (BP) which were shown to yield the best magnetic resonance parameters of the pure generalized gradient approximation (GGA).[39] The basis sets are essentially Slater type with relativistic ZORA/TZ2P, characterized by a core double-ζ, valence triple-ζ and doubly polarized basis. The SOMO was drawn by MOLEKEL4.3.[40]

Acknowledgment. This work was supported by the National Science Council (Taiwan). We gratefully acknowledge Prof. Hong-Chang Yang, Instrumentation Center, for the magnetic measurements, and the Synchrotron Radiation Research Center for X-ray absorption experiments.

Supporting Information Available: X-ray crystallographic data in CIF format for the structure determinations of *trans*-[PPN][Ni(−SeC_6H_4-*o*-NH−$)_2$], *cis*-[PPN][Ni(−TeC_6H_4-*o*-NH−$)_2$], and *trans*-[PPN][Ni(−SC_6H_4-*o*-NH−$)_2$]. This material is available free of charge via the Internet at http://pubs.acs.org.

IC034211R

(32) Sheldrick, G. M. *SADABS, Siemens Area Detector Absorption Correction Program*; University of Göttingen: Göttingen, Germany, 1996.
(33) Sheldrick, G. M. *SHELXTL, Program for Crystal Structure Determination*; Siemens Analytical X-ray Instruments Inc.: Madison, WI, 1994.
(34) (a) te Velde, G.; Bickelhaupt, F. M.; van Gisbergen, S. J. A.; Guerra, C. F.; Baerends, E. J.; Snijders, J. G.; Ziegler, T. *J. Comput. Chem.* **1999**, *22*, 931. (b) Guerra, C. F.; Snijders, J. G.; te Velde, G.; Baerends, E. J. *Theor. Chem. Acc.* **1998**, *99*, 391. (c) *ADF2002.02*; SCM Theoretical Chemistry, Vrije Universiteit: Amsterdam, The Netherlands; http://www.scm.com.
(35) (a) Chang, C.; Pelissier, M.; Durand, M. *Phys. Scr.* **1986**, *34*, 394. (b) van Lenthe, E.; Baerends, E. J.; Snijders, J. G. *J. Chem. Phys.* **1993**, *99*, 4597. (c) van Lenthe, E.; Baerends, E. J.; Snijders, J. G. *J. Chem. Phys.* **1994,** *101*, 9783. (d) van Lenthe, E.; van Leeuwen, R.; Baerends, E. J.; Snijders, J. G. *Int. J. Quantum Chem*. **1996**, *57*, 281.
(36) Vosko, S. H.; Wilk, L.; Nusair, M. *Can. J. Phys.* **1980**, *58*, 1200.
(37) (a) Becke, A. D. *J. Chem. Phys.* **1986**, *84*, 4524. (b) Becke, A. D. *Phys. Rev.* **1988**, *A38*, 3098.
(38) (a) Perdew, J. P. *Phys. Rev*. **1986**, *B33*, 8822. (b) Perdew, J. P. *Phys. Rev.* **1986**, *B34*, 7406.
(39) Belanzoni, P.; Baerends, E. J.; Gribnau, M. *J. Phys. Chem. A* **1999**, *103*, 3732.
(40) Flükiger, P.; Luthi, H. P.; Portmann, S.; Weber, J. *Molekel4.3*; Swiss Center for Scientific Computing: Manno, Switzerland, 2000−2002.